Adsorbate Effects on Structure and Shape of Supported Nanoclusters: A Molecular Dynamics Study

Eduardo J. Lamas and Perla B. Balbuena*

Department of Chemical Engineering, University of South Carolina, Columbia, South Carolina 29208

Received: January 29, 2003; In Final Form: May 20, 2003

Classical molecular dynamics simulations are used to examine the effects of adsorption of inert-gas atoms (Ar, Xe, and He) at various pressures and temperatures on the shape, structure, and diffusion of a 256-atom platinum nanocluster supported on a graphite substrate. The many-body Sutton Chen potential is used to model the Pt−Pt interactions, and the Lennard-Jones potential is employed for the rest of the pair interactions. Gas adsorption on the metal cluster is monitored as a function of pressure at constant temperature, and the evolution of the structure is analyzed as the pressure is increased and then as the gas phase is gradually removed. It is found that the gas phase substantially alters the vacuum cluster structure, and the changes are mostly irreversible in the time frame of the simulations (2 ns), especially at temperatures well below the cluster melting point, where the low energy structures determined under high pressures are very stable. The dynamic properties are also modified by the gas phase; the cluster diffusion depends on the inert gas pressure, being lower at high gas pressures. Although the contact area cluster−substrate is significantly smaller compared to the vacuum case, the size mismatch is reduced because of the presence of the gas-adsorbed layer that forces the rearrangement of the metal atoms leading to distorted structures which favor the Pt−C interactions.

1. Introduction

Supported Pt nanoclusters are used in many technological applications, such as catalysts in the chemical industry,[1−3] in environmental catalysis applications,[4,5] and as catalysts and electrocatalysts for fuel cells.[6,7] In these applications, the metallic cluster is working under conditions of pressure, temperature, and environment, dramatically different from those where most common experimental surface science characterization techniques are applicable.[8−11] However, recent experiments have been able to determine metallic nanocluster structural and dynamic properties under more realistic conditions.[12] Graoui et al.[13] investigated the structural changes taking place in Pd particles exposed to oxygen at high temperatures, observing the particles ex situ via high-resolution electron microscopy (HRTEM) and weak beam dark field (WBDF) imaging. They found that shape changes induced after exposing Pd clusters to oxidizing environments at around 550 °C are reversible after being under a reducing atmosphere. It was concluded that if the temperature is high enough to enable surface atoms diffusion the cluster recovers its original equilibrium structure. Hansen et al.[8] using in situ TEM found that the structure of Cu nanoparticles is influenced by both the nature of the support and by that of the gaseous environment and that reversible changes are strongly dependent on the nature of the gas phase. Other studies[14] reported images obtained with scanning tunneling microscopy which reflected changes induced by the presence of oxygen and nitrogen oxide over Pd nanocrystals, revealing changes in the nanocrystal surface. These shape changes modify the surface structure, and the nature of the exposed sites, therefore altering the cluster catalytic activity.

From these preliminary experiments, it can be concluded that the presence of adsorbed atoms exerts a significant effect on the nanocluster surface atoms, having an impact in the overall cluster structure due to the high ratio of surface to bulk atoms present in nanoparticles. However, several open questions remain regarding the detailed influence of the combined pressure/temperature effect on the catalytic activity of the nanoparticles. At nanoscale lengths, ab initio quantum and classical atomistic and molecular simulations provide insights that in conjunction with experimental studies yield a more complete description of physical phenomena.[15−18] Here we report a systematic classical molecular dynamics (MD) study of the pressure effect exerted by Ar, He, and Xe environments on a 256-atom Pt nanocluster at various temperatures.

2. Methodology

2.1. MD Procedure. Classical MD simulations are used to analyze the gas-phase effects on the physical properties of the metal nanoclusters. Each particle is treated as a point mass, and the motion is governed by Newton's second law; the thermodynamic and transport properties are obtained from time averages over the ensemble of particles.[19,20] The canonical NVT ensemble was sampled using the Evans thermostat.[21] A (42.6 × 49.2 × 60) Å^3 cell of parallelepiped geometry was used in the simulations, with periodic boundary conditions imposed in the *x*, *y*, and *z* directions and temperatures in the range from 200 to 1100 K. The equations of motion were integrated using the Verlet leapfrog method with a time step of 0.001 ps. The simulations reported here were done for a 256-atom Pt cluster supported over a fixed graphite substrate, modeled as two carbon layers arranged in the AB configuration. The selection of the cluster size was based on the availability of many structural and dynamic properties reported in previous work.[22] The cluster diameter, estimated in 1.7 nm, is in the range of particle sizes of interest for catalytic and electrocatalytic processes.[1,2,6]

A cube-shaped fcc cluster arranged in a sequence of (111) layers parallel to the substrate was located at about 3.4 Å above

* To whom correspondence should be addressed. E-mail: balbuena@engr.sc.edu.

10.1021/jp034233z CCC: $25.00
Published on Web 09/30/2003

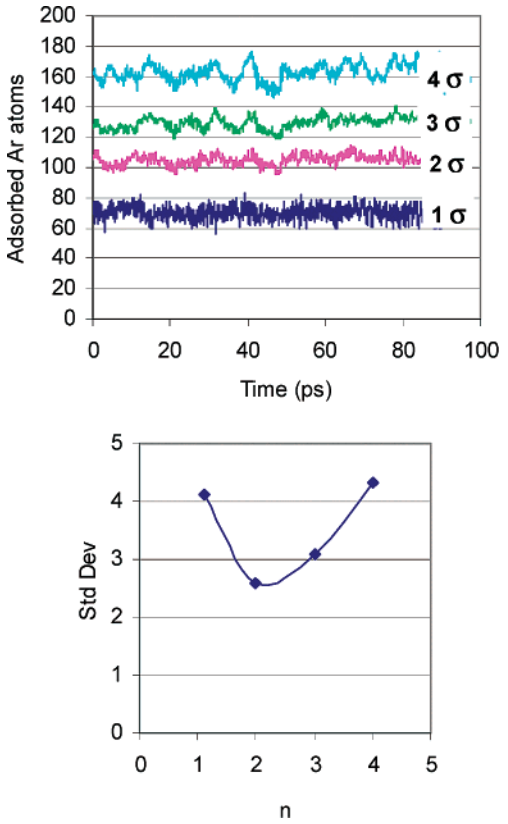

Figure 1. Illustration of the criteria used to determine the adsorption distance. Top: Time evolution of the number of adsorbed atoms at distances $n\sigma$ ($n = 1-4$), where σ is the metal-gas Lennard-Jones parameter. Bottom: Standard deviation corresponding to the various values of n ($T = 200$ K with 361 Ar load).

the graphite surface and used as the initial configuration in most of the simulations, except in the cases when the gas atmosphere was gradually removed, in which the initial structure was the one equilibrated at the immediately previous conditions. The gas-phase atoms were initially randomly distributed in the cell. Simulation lengths of 800 ps for stabilization were followed by 300 ps of production time. The pressure was decreased at constant temperature in the system by extracting some Ar atoms (about 10% of the total load) and continuing the runs by adding 100 ps of stabilization time followed by 300 ps of production time. The evolution of the structure was followed as a function of these state conditions. Three inert gases were used to represent the gas pressure, Ar, Xe, and He. All of the simulations were made using the DL_POLY program.[23]

Adsorption was calculated considering as adsorbed any atom located at a distance equal or lower than $2^*\sigma$ where σ is the metal-gas Lennard-Jones (LJ) parameter. Such adsorption distance was adopted based on the minimum standard deviation calculated for the variation in the number of adsorbed atoms vs time at various gas-metal distances $n\sigma$ ($n = 1-4$) as depicted in Figure 1. Large fluctuations are observed at small distances ($n = 1$), indicating that an adsorbed atom strongly vibrates within a certain equilibrium distance. On the other hand, gas atoms located at longer distances ($n \geq 3$) resemble the behavior of free molecules in the gas phase therefore resulting in larger fluctuations. Analyzing the fluctuations observed at varying adsorbing distances, we have chosen the one ($n = 2$) that gives the smallest fluctuations.

In addition, as an indicator of phase change on the metal cluster, we studied the structural features that the cluster exhibits when is in a liquid or in a solid state. Thus, the cluster structure was analyzed by the time evolution of the following parameters obtained from the calculation of average instantaneous distances to the cluster center of mass:

$$\eta_q(t) = \frac{1}{N_{Pt}} \sum_{i=1}^{N_{Pt}} |q_i(t) - q_{cm}(t)| \quad (1)$$

$$R(t) = \frac{1}{N_{Pt}} \sum_{i=1}^{N_{Pt}} [(x_i(t) - x_{cm}(t))^2 + (y_i(t) - y_{cm}(t))^2 + (z_i(t) - z_{cm}(t))^2]^{1/2} \quad (2)$$

where N_{Pt} is the total number of Pt atoms, q_i is the coordinate of the i atom in the x, y, or z direction, and q_{cm} is the coordinate corresponding to the cluster center of mass.

The atomic number distribution $N(z)$, with the z axis perpendicular to the substrate plane, is defined as

$$N(z) = \langle \sum_{i=1}^{N_{Pt}} \delta(z_i - z) \rangle \quad (3)$$

where the brackets represent the time average.

The self-diffusion coefficient D for the whole cluster is obtained from the 2-dimensional square displacement

$$D = \frac{1}{4\Delta t} \langle |(r_{cm}(t+s) - r_{cm}(s)|^2 \rangle \quad (4)$$

where $r_{cm}(t + s)$ is the vector position of the cluster center of mass on the xy plane and the average is over choices of the time origin s.

2.2. Potential Functions. The interactions in the metal cluster were modeled with the Sutton-Chen (SC) many body potential. The use of an effective potential such as the SC model has advantages such as ease of programming and low computation times, which permit the investigation of relatively long-time phenomena, such as cluster diffusion. This potential model describes reliably static and dynamic properties of transition and noble metals, such as bulk moduli and elastic constants,[24] as well as surface energies, stress tensor components, and surface relaxation of fcc metals.[25] Although developed for bulk metals, the SC model has been applied to optimize the structure of transition metal clusters and search for the global minima in Monte Carlo simulations,[26] and the most stable structures found in these studies are in good agreement with experimental observations. The SC potential model can be written as

$$U_{tot} = \epsilon_{SC} \left[\frac{1}{2} \sum_{i \neq j} \sum \left(\frac{a}{r_{ij}} \right)^n - c \sum_i \sqrt{\rho_i} \right] \quad (5)$$

The first term in eq 5 is a pairwise repulsive potential and the second term represents the metallic bonding energy associated with the local electron density ρ_i, defined as

$$\rho_i = \sum_{j \neq i} \left(\frac{a}{r_{ij}} \right)^m \quad (6)$$

Here r_{ij} is the distance between atoms i and j, c is a dimensionless parameter, ϵ_{SC} is a parameter with the dimensions of energy, and a is the fcc lattice constant. For Pt, the SC parameters are $\epsilon_{SC} = 0.01983$ eV, $c = 34.408$, $a = 3.92$ A, $n = 10$, and $m = 8$.[24]

For the rest of the interactions, which are relatively weaker, we used the 12−6 LJ potential, with the parameters listed in

TABLE 1: Lennard-Jones Parameters for C−C, C−Gas, Metal−Gas, and Gas−Gas Interactions[a]

interaction	ϵ (eV)	σ (Å)	interaction	ϵ (eV)	σ (Å)
Pt−Pt [ref 27]	0.2013	2.41	Ar−Ar [ref 36]	0.0080	3.54
Pt−C	0.0220	2.90	Ar−Pt	0.0402	2.98
C−C [ref 27]	0.0024	3.40	Ar−C	0.0044	3.47
He−He [ref 36]	0.0009	2.55	Xe−Xe [ref 36]	0.0199	4.05
He−Pt	0.0133	2.48	Xe−Pt	0.0633	3.23
He−C	0.0015	2.97	Xe−C	0.0693	3.72

[a] The Pt−Pt parameters are used only to calculate the cross Pt−X interactions using Lorentz−Berthelot rules. The Pt−Pt interaction is described by the Sutton−Chen potential (see text).

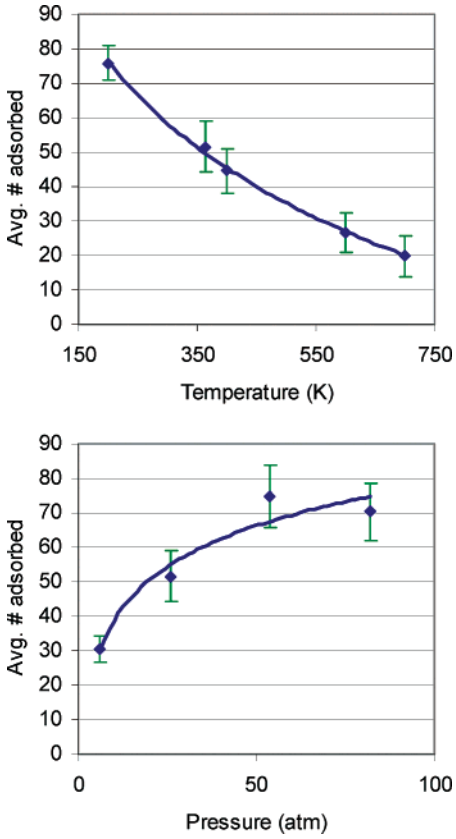

Figure 2. Top: Adsorption at various temperatures (constant Ar load = 144 Ar atoms). Bottom: Adsorption isotherm at 363 K, where the gas pressure is estimated according to the ideal-gas law. Error bars are estimated such that 95% of the adsorbed atoms are within the indicated range at each point.

Table 1.[19] Reported values[27] of an effective LJ potential to represent the Pt−Pt interactions were used to calculate the parameters for C−Pt interactions using the Lorentz Berthelot mixing rules. To reduce the computational load, here we only consider a static substrate, fixing the positions of the C atoms in all simulations.

3. Results and Discussion

3.1. Adsorption. Figure 2 (top) displays the temperature dependence of the number of adsorbed Ar atoms on the Pt nanocluster, under a constant Ar load of 144 Ar atoms in the unit cell of volume 125778.82 Å^3. The number of adsorbed atoms decays almost exponentially when the temperature increases and becomes considerably reduced at temperatures close to the nanocluster melting point (~1020 K).[22] Figure 2 (bottom) illustrates the pressure dependence of the number of adsorbed Ar atoms at 363 K. The adsorption isotherm responds to Langmuir type I in the IUPAC classification[28] where, above a certain load, adsorption reaches its saturation coverage. The adsorption process is dominated by the dynamics of the adsorbed atoms and by interactions among them, with the cluster, and with the substrate; the structure of the adsorbed layer is further discussed in a later section. Based on the values of the gas-metal interaction energy and size LJ parameters adsorption is expected to decay in the order Xe > Ar > He. However, at low temperatures, more Ar atoms can be accommodated because of their smaller size. For example, at 200 K, the average number of adsorbed atoms is 110 for Ar, 98 for Xe, and 50 for He, whereas at 363 K, because of desorption effects, the behavior reverts to the expected: Xe (90 atoms) > Ar (80 atoms) > He (30 atoms).

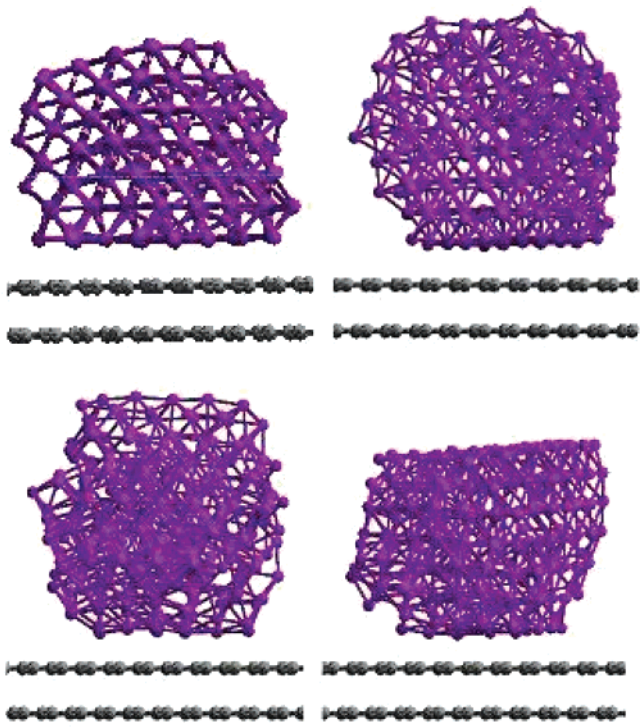

Figure 3. Pt-cluster structures. Top left: In a vacuum at 363 K. Bottom left: At 363 K with 361 Ar atoms. Top right: The vacuum structure obtained after gradually reducing the gas pressure from a value of 361 to zero Ar atoms, at 363 K. Bottom right: At 200 K with 361 Ar atoms. The Ar atoms were deleted for clarity.

3.2. Effect of the Gas Phase on Cluster Structure. Figure 3 shows snapshots of the 256-atom supported Pt cluster under vacuum (top left) and the same cluster under an Ar atmosphere constituted by 361 Ar atoms in a volume of 125 778.82 Å^3 (bottom left), where the gas molecules have been deleted for clarity. In contrast to the layered structure at the vacuum conditions (Figure 3, top left), the cluster under pressure at 363 K (Figure 3, bottom left) shows an expansion in the z direction perpendicular to the graphite substrate, and the core of the cluster shows an amorphous structure, revealing an intense atomic motion. When the pressure is gradually reduced back to zero, at 363 K (Figure 3, top right), the cluster evolves to a structure that is qualitatively comparable to the one observed in a vacuum indicating a small degree of reversibility at this temperature upon the pressure change. The irreversibility is more pronounced if the process of pressure reduction is implemented at a lower temperature. The cluster does not revert to its original structure, and this stable structure is shown in Figure 3, bottom right, at 200 K.

Thus, at a given cluster size, the impact of the gas phase on the cluster depends on coverage, temperature, and nature of the

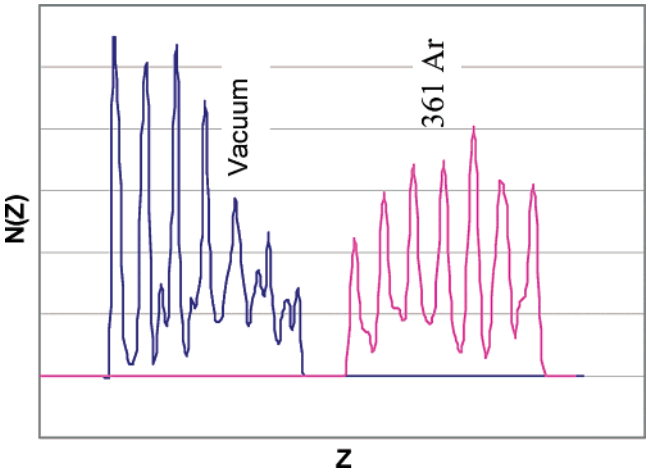

Figure 4. Density profile in a direction (*z*) perpendicular to the substrate, for the Pt cluster in a vacuum and under pressure exerted by 361 Ar atoms, at 200 K. The substrate is located at the left of each of these density profiles.

gas. For all gases in this study, the interaction between the gas and the metal tends to stabilize the surface atoms on the metal cluster, in agreement with reported experimental observations and theoretical calculations. The structural changes are easily revealed by the *z*-density profiles, as illustrated in Figure 4. The metal cluster surface atoms are redistributed in order to favor the interactions with the gas-phase atoms and with the substrate driving the cluster to a lower energy state. In general, the metal layer in contact with the substrate becomes smaller, the cluster adopts a more rounded shape, and sometimes new layers appear in the direction perpendicular to the substrate, in good agreement with other theoretical studies that predict similar structural changes in nanoparticles even at low coverages.[29] A comparison of the cluster layer in contact with graphite with and without the gas phase (Figure 5) indicates how this layer (Figure 5, bottom) becomes highly distorted with respect to the initial (111) structure, and also it is substantially reduced, as was noted in the density profile (Figure 4, right). Some of the Pt atoms on this layer arrange in almost perfectly curved lines in an effort to maximize the interactions with the graphite lattice and those with adsorbed Ar atoms, the latter in most cases are found in the center of the aromatic rings. Scanning tunneling microscopy (STM) studies of 2-dimensional Pt islands and 3-dimensional clusters deposited on highly oriented pyrolytic graphite (HOPG)[30] have suggested that Pt atoms in contact with the substrate may tend to align with the underlying carbon atoms, occupying either $\beta-\beta$ sites separated 2.46 Å or bridge sites connecting first neighbors in the graphite hexagonal structure. Rotations of 20−30° of the Pt layer with respect to the orientation of the substrate were also found by the same STM studies, whereas others[31,32] detected well-defined rectangular (rather than close packed) lattices, incommensurate with the substrate, for Ag islands deposited on graphite. Our calculated structures (Figure 5) show evidence of an evolution toward the formation of rectangular lattices, presumably a most stable configuration because it tends to maximize the interactions with the C atoms, where the Pt atoms mostly locate on β sites. Such conformational evolution of the contact layer is favored by the presence of the gas phase (Figure 5, bottom).

Figure 6 illustrates the structure of the adsorbed gas layer, and the interactions with the substrate at 200 K under a gas atmosphere exerted by 361 Ar atoms. Each Ar atom interacts with two Pt atoms (on the average), as can be observed in the sequence of layers (1−7) shown in Figure 6, and in most cases,

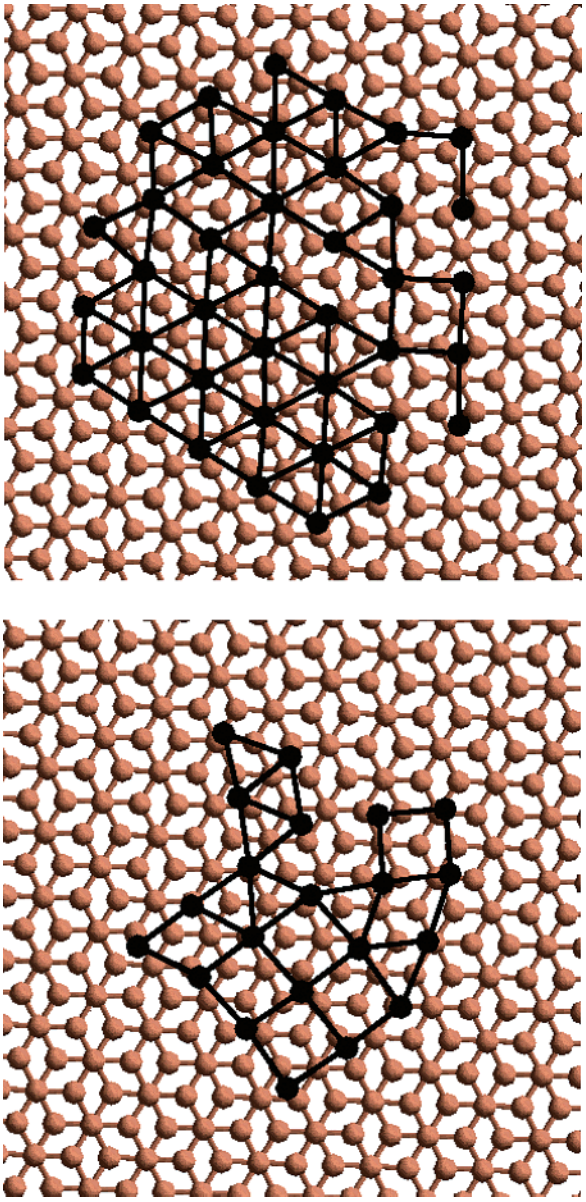

Figure 5. Top: Structure of the Pt cluster layer in contact with the graphite substrate at 200 K in a vacuum. Bottom: Same with 361 Ar atoms (not shown).

a bridge-type coordination is found between the Ar atoms and the Pt atoms located at the perimeter of each layer. The adsorbed layer is very ordered; each Ar atom adsorbs in close coordination with its closest Pt atoms, despite the dynamic equilibrium prevalent at finite temperatures. A one-to-one Ar−Pt coordination is observed on the top layer, arranged in a regular pattern over the Pt layer, which is the one where the cluster atoms best retain the (111) structure. The image of the top layer (layer 7) also shows evidence of the development of a full monolayer on the (111) surface at 200 K.

The other type of structural change observed from our simulations may be characterized by the evolution of the cluster *z*-density profile upon gradual removal of the gas atmosphere, shown in Figure 7. The process followed to obtain the structures in Figure 7 started with equilibration of the supported metal cluster under high-pressure conditions, yielding a disordered structure, and then pressure was gradually reduced (as explained in the methodology section) starting from the previous equilibrated structure. The internally disordered structure found at relatively high temperatures (363 K in Figure 7), when the

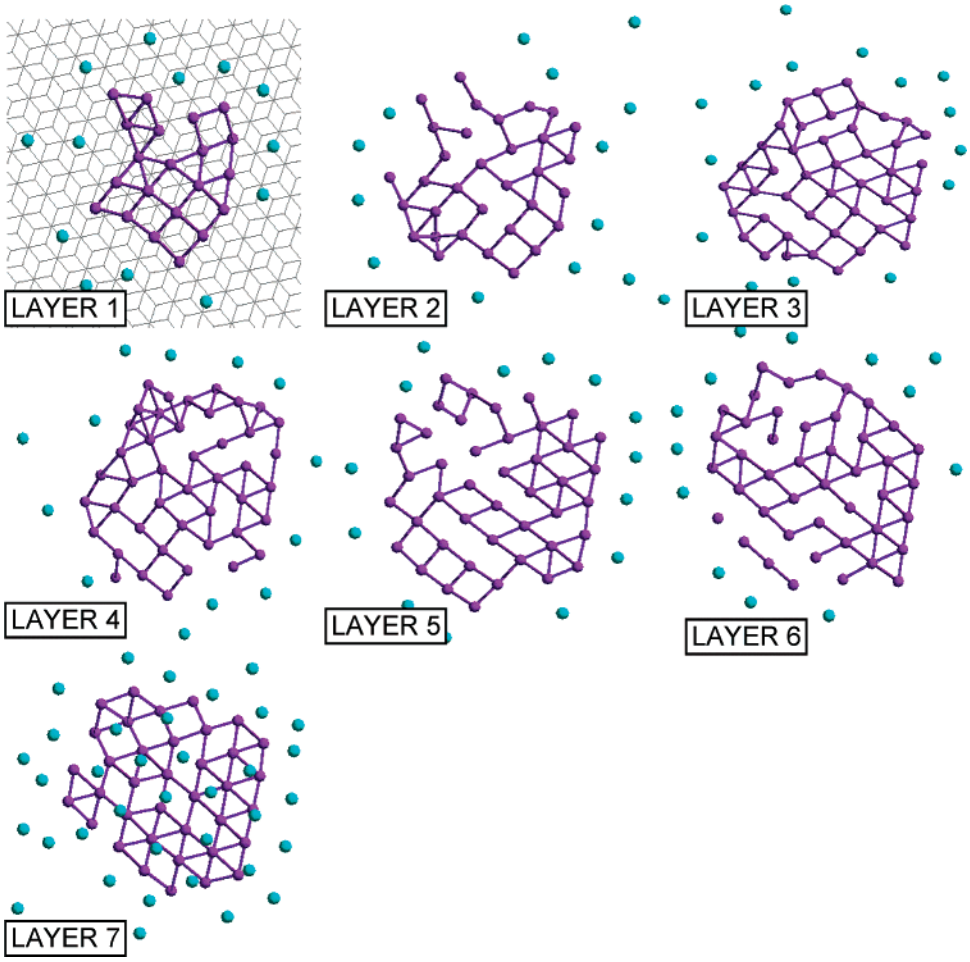

Figure 6. Layer-by-layer structure for the cluster exposed to 361 Ar atoms, at 200 K. Layers are numbered starting with the one in contact with the graphite layer. Ar atoms in the first shell surrounding each of the cluster layers are displayed.

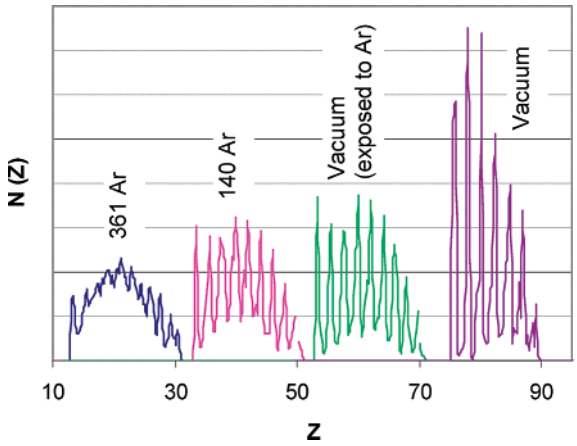

Figure 7. Metal cluster structural evolution when the gas pressure is reduced from a disordered initial structure, at 363 K. The substrate is located at the left of each of these density profiles.

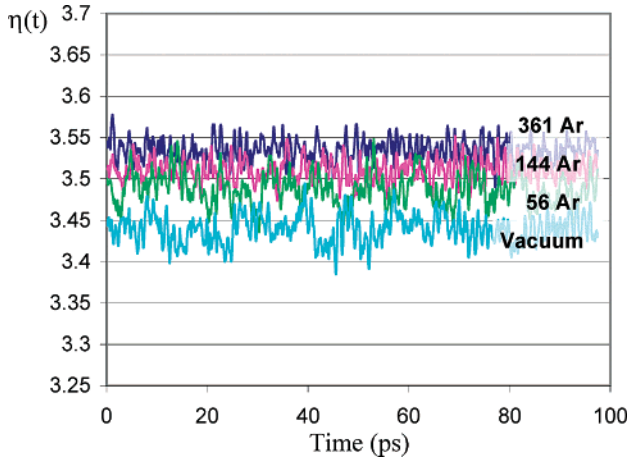

Figure 8. Elongation effect in the direction perpendicular to the substrate, evidenced by the deformation parameter (eq 1) in the z direction, for the cluster under various pressures at $T = 363$ K. All simulations started from the same initial conditions as indicated in the text.

cluster is under the gas phase, is a local minimum in the configurational energy space as indicated by the values of the calculated energy for the isolated cluster (excluding all the other external interactions: gas phase and substrate) which were very similar to those of the layered vacuum structure at the same temperature. The more rounded shape observed in the cluster (Figure 7, first from left) probably compensates the internal stress associated with the lack of structure as it was discussed in relation to energy minimization of small unsupported clusters in a vacuum.[26] We studied the cluster stability for the amorphous structure in Figure 7 (left) using longer simulation times and found that after extending the simulation time for another 500 ps the structure remained stable.

The shape of the cluster when the pressure is decreased at constant temperature (Figure 7) evolves from an amorphous to a layered structure, which, as discussed before, is still different from the structure obtained in vacuum simulations, showing that, even after some relaxation upon removal of the gas phase, the

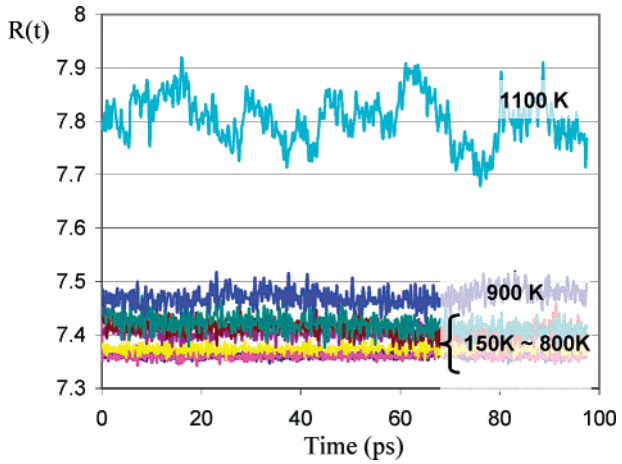

Figure 9. Deformation parameter in the *R* direction, given by eq 2, used as an indicator of cluster melting transition.

atomic diffusion in the metal cluster is not high enough to allow the cluster to recover its original vacuum structure in the time frame of these simulations (2 ns). The nonreversibility effect is more pronounced at low temperatures, where the metal cluster exposed to a gas phase adopts a layered structure, such as that shown in Figure 3 (bottom, right), at 200 K, which is very stable, retaining its morphology when the pressure is gradually reduced until vacuum.

The calculated deformation parameters $\eta(t)$ in the *z* direction (Figure 8), defined by eq 1, are also indicators of the cluster shape evolution. Thus, at constant temperature ($T = 363$ K), the average value of η (in the *z* direction) increases as pressure increases, as revealed by elongations and formation of new layers in the direction perpendicular to the substrate, as observed in the corresponding density profile, shown in Figure 7. Such vertical elongation is a consequence of compression on the lateral surfaces because of the adsorbed gas, and it is clearer at relatively high temperatures where the cluster atomic motion is more intense. Note that, as the number of atoms in the gas phase increases, $\eta(t)$ tends to a constant value because of surface saturation.

The deformation parameter $R(t)$ defined by eq 2 is also an indicator for the detection of phase transitions in the cluster, as illustrated by Figure 9. The distinct dynamical behavior of the cluster structure in the liquid and solid phases is clear from this figure. In the liquid state (at 1100 K), the shape variation of the cluster as a function of time is much more noticeable and lower-frequency oscillations can be noted. The calculated melting point of this cluster is about 1020 K.[22]

3.3. Cluster Diffusion. The dynamics of diffusion of the metal cluster over the graphite layers is much slower than that of the other properties analyzed in this work, and therefore, much longer simulation times are required. The simulations were run during a total time of 2.1 ns with a stabilization time of 800 ps, and the history file was stored during the last 1.1 ns. Those times were enough to evaluate the cluster motion and calculate its associated properties.

However, even when the diffusion occurs in a long time frame (compared with other phenomena studied in the previous sections), conformational changes driven by atomic vibrations in the short time scale are the ones that originate the various forces cluster−substrate that result in the cluster movement. It was observed that the cluster structure changes in the short time scale as illustrated by the time evolution of the deformation parameters that reveal the dynamics of the structural changes on the cluster. Even when cluster motion is not yet observable in the time frame where these intense atomic vibrations occur, they are responsible for the temperature dependence on the cluster diffusion.

We identify two types of forces acting on the cluster dynamics. The first one is a group of forces among the atoms in the cluster itself associated with atomic vibrations. This net force should be zero because it is the result of an internal motion which cannot induce motion of the cluster center of mass. The second group of forces is that acting on the cluster atoms due to the force field that arises from the interaction cluster−substrate, and the component of this force on the *xy* plane is originated on the cluster−substrate atomic mismatch[33] (see for example Figure 5); these forces are variable in nature because of the dynamical change in the cluster structure originated from the internal forces. The cluster−substrate dynamical forces are expected to be functions of the strength of the interaction cluster−surface, of the extent of the cluster−substrate interfacial contact area, as well as of the structural variations on the cluster

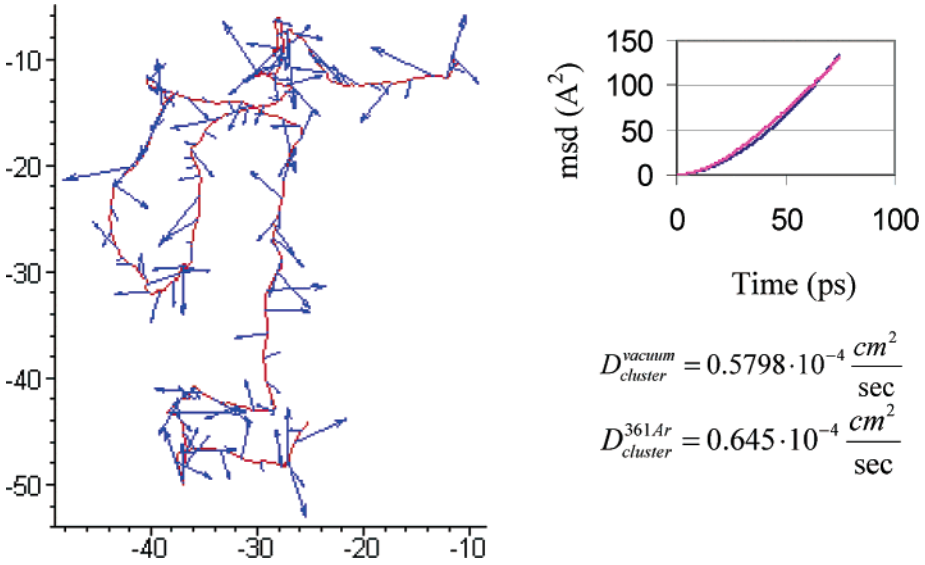

Figure 10. *X* and *Y* coordinates of the cluster center of mass in a vacuum at 1100 K. The arrows represent the forces acting on the cluster center of mass at each time. Inset: Mean square displacement (msd) and diffusivities for the cluster center of mass at the same temperature in a vacuum and with 361 Ar atoms.

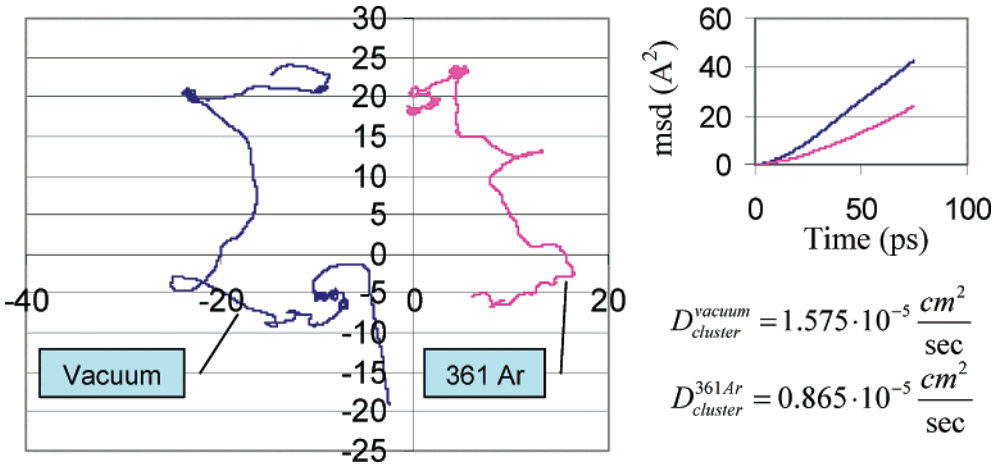

Figure 11. *X* and *Y* coordinates of the cluster center of mass in a vacuum and in the presence of 361 Ar atoms at 500 K. Inset: Mean square displacement and diffusivities for the cluster center of mass.

surfaces due to its intrinsic (temperature-driven) atomic motion. As a result, a net force arises which determines the cluster motion on the surface. We have calculated the cluster−substrate forces in the *xy* plane corresponding to the layer in contact with the substrate; these forces are shown as functions of the positions of the cluster center of mass at 1100 K in a vacuum (Figure 10). The indicated length is proportional to the magnitude of the force at each point. Figure 10 shows that a sequence of relatively small forces is followed by a large force, which appears at a frequency of 10−20 ps at 1100 K, revealing an intense atomic motion that at this temperature is not affected by the gas phase. Thus, above the cluster melting point, where gas adsorption is negligible, and therefore the cluster structure is similar in a vacuum and under pressure, the presence of the gas phase has practically no effect on the cluster motion, and no differences are found between the calculated cluster diffusion coefficient in a vacuum and in the presence of the gas phase.

More striking are the results at lower temperatures (for example at 500 K, Figure 11) where the effect of the gas phase is evident. In this case, the vacuum cluster structure is different than that observed under pressure, and as it was mentioned in relation to the structural analysis, the wetting layer for the cluster under pressure is smaller, and therefore, the modified interaction with the substrate gives rise to a different diffusivity. The calculated values for the diffusivity of the Pt nanocluster in a vacuum are in good agreement with the reported value[34] for a gold cluster under similar conditions (500 K and vacuum), $D = 1.09 \times 10^{-5}$ cm^2/s for a 249 atoms cluster, while our calculations yield $D = 1.575 \times 10^{-5}$ cm^2/s, whereas the value of the cluster diffusion under pressure is reduced practically to half its value in a vacuum. As extensively discussed in the literature,[33−35] when the cluster and the substrate are commensurate, epitaxial locking may occur. At low temperatures (as in Figure 5), the cluster atoms are constrained to their equilibrium positions and cannot easily adjust to the substrate potential.[33] Even though, at 200 K, in a vacuum, some rearrangement of the perimeter atoms is observed, where the Pt atoms tend to distribute according to a rectangular lattice, and as discussed above in relation to Figure 5, such distribution is enhanced under the gas phase.

Figure 12 illustrates the structure of the cluster layer in contact with the substrate at 500 K in a vacuum and under a 361 Ar atoms atmosphere. At this temperature, the atomic redistribution in the cluster layer in contact with the substrate is much more pronounced, and bond elongations are clearly observed. The gas phase (Figure 12, bottom) induces the atomic redistribution

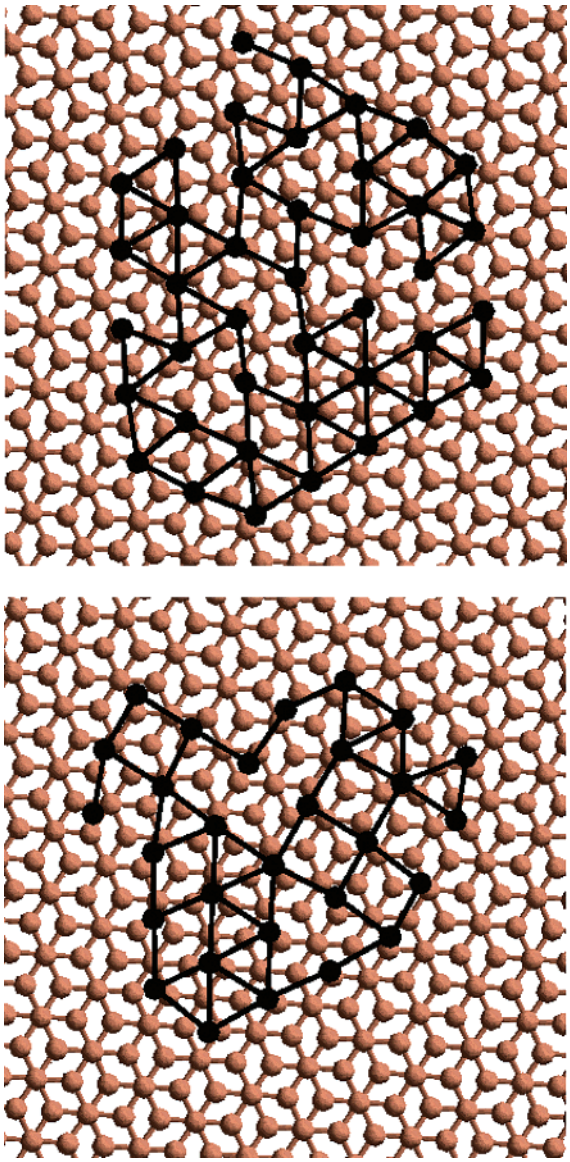

Figure 12. Top: Structure of the Pt cluster layer in contact with graphite at 500 K in a vacuum. Bottom: Same with 361 Ar atoms (not shown). The effect of the gas phase is to reduce the cluster-substrate mismatch, maximizing the favorable Pt−C interactions in a smaller wetting layer.

in the cluster that effectively reduces the cluster−substrate mismatch, at the same time that the gas-phase atoms occupy energetically favorable positions interacting both with the cluster and with the substrate, thus slowing down cluster diffusion. The gas phase-induced reduction of the area of the wetting layer (Figures 5 and 12) is another factor that favors the slower motion of the cluster, because of the consequent decrease of the effective driving force for such motion.

4. Conclusions

The analysis of the structure of a Pt nanocluster under an inert gas atmosphere indicates that the presence of adsorbed molecules stabilizes the surface cluster atoms changing the atomic distribution in the whole cluster.

At low temperatures ($T < 300$ K), the structural change results in a modified layered structure, which remains practically unaltered even after the gas phase has been removed. At higher temperatures, the metal cluster under a gas phase adopts an amorphous conformation, which gradually evolves to a layered structure (different from that in a vacuum) as the gas pressure is reduced. In all cases, the structural changes due to the presence of the gas phase were found to be not completely reversible.

The size of the cluster layer in contact with the substrate is substantially reduced under the gas-phase atmosphere, and the cluster atoms in that layer evolve from the (111) structure to rearrange in rectangular lattices. The gas phase also causes elongations of the cluster in the direction perpendicular to the substrate. The adsorbed layer at low temperatures is well ordered; the inert gas atoms coordinate in a bridge position with the Pt atoms in the perimeter of each cluster layer, whereas the Ar atoms adsorbed on the top (111) surface show a one-to-one coordination Pt−Ar with the development of a full monolayer under these conditions.

The gas phase also alters the cluster dynamical properties if the temperature is low enough so that the presence of the gas can modify the metal cluster structure and therefore its dynamical behavior. At 500 K, the Pt cluster diffusion coefficient is found lower at higher pressure than in a vacuum, this effect is a consequence of the cluster−substrate mismatch reduction induced by the inert-gas atoms that causes the redistribution of the Pt atoms in the contact layer maximizing the favorable Pt−C interactions.

Acknowledgment. This work is supported by the National Science Foundation Career Award Grant CTS-9876065, by the Army Research Office Grant No. DAAD19-00-1-0087, and by the Department of Energy/Basic Energy Sciences, Grant DE-FG02-1ER15249. The use of computational facilities at the National Energy Research Scientific Computing Center, NERSC, and at the Major Shared Resource Center (ARL MSRC) is gratefully acknowledged.

References and Notes

(1) Rachmady, W.; Vannice, M. A. Acetic Acid Hydrogenation over Supported Platinum Catalysts. *J. Catal.* **2000**, *192*, 322.

(2) Bazin, D. Solid-state concepts to understand catalysis using nanoscale metallic particles. *Top. Catal.* **2002**, *18*, 79.

(3) Bazin, D.; Mottet, C.; Treglia, G.; Lynch, J. New trends in heterogeneous catalysis processes on metallic clusters from synchrotron radiation and theoretical studies. *Appl. Surf. Sci.* **2000**, *164*, 140.

(4) Bergels, J.; Kasemo, B.; Chakarov, D. V. CO oxidation on Pt(111) promoted by coadsorbed H_20. *Surf. Sci. Lett.* **2001**, *495*, L815.

(5) Papaefthimiou, P.; Ioannides, T.; Verykios, X. E. VOC removal: investigation of ethyl acetate oxidation over supported Pt catalysts. *Catal. Today* **1999**, *54*, 81.

(6) Adzic, R. Recent advances in the kinetics of oxygen reduction. In *Electrocatalysis*; Lipkowski, J., Ross, P. N., Eds.; Wiley-VCH: New York, 1998; p 197.

(7) Mehta, V.; Cooper, J. S. Review and analysis of PEM fuel cell design and manufacturing. *J. Power Sources* **2002**, *5044*, 1.

(8) Hansen, P. L.; Wagner, J. B.; Helveg, S.; Rostrup-Nielsen, J. R.; Clausen, B. S.; Topsoe, H. Atom-Resoved Imaging of Dynamic Shape Changes in Supported Copper Nanocrystals. *Science* **2002**, *195*.

(9) El-Sayed, M. Some interesting properties of metals confined in time and nanometer space of different shapes. *Acc. Chem. Res.* **2001**, *34*, 257.

(10) Somorjai, G. A. *Introduction to Surface Chemistry and Catalysis*; John Wiley & Sons: New York, 1994.

(11) Freund, H. J. Introductory Lecture: Oxide surfaces. *Faraday Discuss.* **1999**, 1.

(12) Bazin, D.; Mottet, C.; Treglia, G. New opportunities to understand heterogeneous catalysis processes on nanoscale bimetallic particles through synchrotron radiation and theoretical studies. *Appl. Catal. A: General* **2000**, *200*, 47.

(13) Graoui, H.; Giorgio, S.; Henry, C. R. Shape variations of Pd particles under oxygen adsorption. *Surf. Sci.* **1998**, *417*, 350.

(14) Hansen, K. H.; Slivancanin, Z.; Laegsgaard, E.; Besenbacher, F.; Stensgaard, I. Adsorption of O_2 and NO on Pd nanocrystals supported on Al_2O_3/NiAl (110): overlayer and edge structures. *Surf. Sci.* **2002**, *505*, 25.

(15) Baletto, F.; Doye, J. P.; Ferrando, R. Evidence of kinetic trapping in clusters of C_{60} molecules. *Phys. Rev. Lett.* **2002**, *88*, 075503.

(16) Baletto, F.; Mottet, C.; Ferrando, R. Reentrant morphology transition in the growth of free silver nanoclusters. *Phys. Rev. Lett.* **2000**, *84*, 5544.

(17) Baletto, F.; Mottet, C.; Ferrando, R. Growth simulations of silver shells on copper and palladium nanoclusters. *Phys. Rev. B* **2002**, *66*, 155420.

(18) Jensen, P. Growth of nanostructures by cluster deposition: Experiments and simple models. *Rev. Mod. Phys.* **1999**, *71*, 1695.

(19) Allen, M. P.; Tildesley, D. J. *Computer Simulation of Liquids*; Oxford University Press: Oxford, 1990.

(20) Frenkel, D.; Smit, B. *Understanding Molecular Simulation: From Algorithms to Applications*; Academic Press: New York, 1996.

(21) Evans, D. J. Computer "experiment" for nonlinear thermodynamics of Couette flow. *J. Chem. Phys.* **1983**, *78*.

(22) Huang, S.-P.; Balbuena, P. B. Platinum Nanoclusters on Graphite Substrates: A Molecular Dynamics Study. *Mol. Phys.* **2002**, *100*, 2165.

(23) Smith, W.; Forester, T. R. DL_POLY; Daresbury Laboratory: Daresbury, 1996.

(24) Sutton, A. P.; Chen, J. Long-range Finnis-Sinclair potentials. *Philos. Mag. Lett.* **1990**, *61*, 139.

(25) Todd, B. D.; Lynden-Bell, R. M. Surface and bulk properties of metals modelled with Sutton−Chen potentials. *Surf. Sci.* **1993**, *281*, 191.

(26) Doye, J. P. K.; Wales, D. J. Global minima for transition metal clusters described by Sutton−Chen potentials. *New J. Chem.* **1998**, 733.

(27) Wu, G.-W.; Chan, K.-Y. Molecular Simulation of Oxygen on Supported Platinum Clusters. *J. Electroanal. Chem.* **1998**, *450*, 225.

(28) Balbuena, P. B.; Gubbins, K. E. Theoretical Interpretation of Adsorption Behavior of Simple Fluids in Slit Pores. *Langmuir* **1993**, *9*, 1801.

(29) Shi, A.-C.; Masel, R. I. The effect of Gas Adsorption on Particle Shapes in Supported Platinum Catalysts. *J. Catal.* **1989**, *120*, 420.

(30) Clark, G. W.; Kesmodel, L. L. Ultrahigh vacuum scanning tunneling microscopy studies of platinum on graphite. *J. Vac. Sci. Technol. B* **1993**, *11*, 131.

(31) Ganz, E.; Sattler, K.; Clarke, J. Scanning tunneling microscopy of Cu, Ag, Au, and Al adatoms, small clusters, and islands on graphite. *Surf. Sci.* **1989**, *219*, 33.

(32) Ganz, E.; Sattler, K.; Clarke, J. Scanning tunneling microscopy of the local atomic structure of two-dimensional gold and silver islands on graphite. *Phys. Rev. Lett.* **1988**, *60*, 1856.

(33) Deltour, P.; Barrat, J.-L.; Jensen, P. Fast diffusion of a Lennard-Jones cluster on a crystalline surface. *Phys. Rev. Lett.* **1997**, *78*, 4597.

(34) Lewis, L. J.; Jensen, P.; Combe, N.; Barrat, J.-L. Diffusion of gold nanoclusters on graphite. *Phys. Rev. B* **2000**, *61*, 16084.

(35) Bardotti, L.; Jensen, P.; Hoareau, A.; Treilleux, M.; Cabaud, B. Experimental observation of fast diffusion of large antimony clusters on graphite surfaces. *Phys. Rev. Lett.* **1995**, *74*, 4694.

(36) Reid, R. C.; Prausnitz, J. M.; Poling, B. E. *The properties of gases and liquids*, 4th ed.; McGraw-Hill: Boston, 1987.